Article

Calcium-Induced Calcium Release during Action Potential Firing in Developing Inner Hair Cells

Radu Iosub,[1] Daniele Avitabile,[3] Lisa Grant,[1] Krasimira Tsaneva-Atanasova,[2] and Helen J. Kennedy[1,*]
[1]School of Physiology and Pharmcology, University of Bristol, Bristol, United Kingdom; [2]Department of Mathematics, College of Engineering, Mathematics and Physical Sciences, University of Exeter, Exeter, United Kingdom; and [3]Centre for Mathematical Medicine and Biology, School of Mathematical Sciences, University of Nottingham, University Park, Nottingham, United Kingdom

ABSTRACT In the mature auditory system, inner hair cells (IHCs) convert sound-induced vibrations into electrical signals that are relayed to the central nervous system via auditory afferents. Before the cochlea can respond to normal sound levels, developing IHCs fire calcium-based action potentials that disappear close to the onset of hearing. Action potential firing triggers transmitter release from the immature IHC that in turn generates experience-independent firing in auditory neurons. These early signaling events are thought to be essential for the organization and development of the auditory system and hair cells. A critical component of the action potential is the rise in intracellular calcium that activates both small conductance potassium channels essential during membrane repolarization, and triggers transmitter release from the cell. Whether this calcium signal is generated by calcium influx or requires calcium-induced calcium release (CICR) is not yet known. IHCs can generate CICR, but to date its physiological role has remained unclear. Here, we used high and low concentrations of ryanodine to block or enhance CICR to determine whether calcium release from intracellular stores affected action potential waveform, interspike interval, or changes in membrane capacitance during development of mouse IHCs. Blocking CICR resulted in mixed action potential waveforms with both brief and prolonged oscillations in membrane potential and intracellular calcium. This mixed behavior is captured well by our mathematical model of IHC electrical activity. We perform two-parameter bifurcation analysis of the model that predicts the dependence of IHCs firing patterns on the level of activation of two parameters, the SK2 channels activation and CICR rate. Our data show that CICR forms an important component of the calcium signal that shapes action potentials and regulates firing patterns, but is not involved directly in triggering exocytosis. These data provide important insights into the calcium signaling mechanisms involved in early developmental processes.

INTRODUCTION

Before the cochlea can respond to sound, developing inner hair cells (IHCs) generate calcium-based action potentials (1) that support position-dependent patterned firing along the length of the cochlea (2). The small conductance (SK2) current, present as early as P0 (3), is critical in triggering the robust repolarization, after hyperpolarization (AHP) and timing of action potential firing (4–8). Although the role of action potential firing has not been fully established it potentially serves two roles; intrinsic hair cell development and guiding central auditory development. It is well established, in other systems, that calcium (Ca^{2+}) signals generated during electrical activity are important in the activation of gene transcription pathways (9–12). Recently, experiments on a mouse overexpressing the SK2 channels demonstrate that changes in the pattern of action potential activity, just before the onset of hearing, prevents the developmental changes in the Ca^{2+} dependence of neurotransmitter release (13). Taken together, this suggests that the early experience-independent firing generates calcium signals that may be important in activating the appropriate gene transcription pathways necessary for the maturation of the hair cell.

In addition, during action potential firing the rises in intracellular calcium trigger transmitter release from immature IHCs (14–16) that drives firing patterns in developing spiral ganglion neurons (17). This type of early developmental experience-independent activity is well established to be important in retinal development (18). By analogy with the visual system, in the auditory system the early electrical activity has been proposed to influence the tonotopic development of the higher auditory pathways (19–21). Thus, the calcium signal generated during action potential firing is likely to be important in the development of both the IHC and higher auditory pathways.

The upstroke of the action potential is generated by calcium influx through Cav1.3 calcium channels (22), resulting in a rise in intracellular calcium. Calcium-induced calcium release (CICR) is an amplification process whereby an increase in intracellular calcium activates calcium release through ryanodine-sensitive channels (RyRs) (23,24). Although CICR is present in developing IHCs (25) its function is unclear.

Here, we investigated whether action potential firing or exocytosis had any dependence on CICR. We used a

Submitted July 1, 2014, and accepted for publication November 26, 2014.

*Correspondence: helen.kennedy@bristol.ac.uk

Editor: Richard Bertram.

0006-3495/15/03/1003/10 $2.00

http://dx.doi.org/10.1016/j.bpj.2014.11.3489

combined approach of experimental measurement of electrical activity or cell capacitance and calcium signals together with mathematical analysis to gain further insight and assess the contributions of CICR to shaping IHCs firing patterns. Our mathematical model (26) explicitly takes into account ion channel characteristics of immature IHCs. During model development, we have given special attention to choosing parameter values within the ranges of published voltage-clamp electrophysiological data (4,7,27). The model includes the main currents found in immature IHCs, and has been validated using current-clamp experimental data (26). In this work, we performed numerical bifurcation analysis of the model and studied the relative contribution of SK2 and CICR in regulation of the calcium signal.

Together, our results show a significant role for CICR in shaping the patterns of electrical activity, but it has no direct role in early exocytosis. By changing the characteristics of the calcium signal, for example through altering CICR, action potential duration and frequency can be changed. These experimental findings are supported by simulations of our IHC biophysical model. Furthermore, performing numerical continuation of the different periodic solutions supported by the model allows us to examine the relative contribution of CICR rate and the amount of SK2 current activated during spiking in shaping action potential pattern and duration.

MATERIALS AND METHODS

All experiments were performed in accordance with United Kingdom Animals (Scientific Procedures) Act (1986) and associated guidelines. Mice (Swiss CD-1) aged between postnatal Day 6 and 11 (P6–P11 where the day of birth is P0) were killed by rapid cervical dislocation and dissected as described previously (25,28).

Electrophysiology

Mid and apical turns of the organ of Corti were excised and mounted in the recording chamber. For all experiments the microscope stage was equipped with a heated stage (built in-house) to maintain the recording chamber at a temperature of 34–37°C. Cells were visualized using the Olympus BX50WI microscope (Olympus, Southend-on-Sea, UK) using a 40× water immersion objective. Cells were continually perfused with an extracellular solution containing (mM): 140 NaCl, 0.7 NaH_2PO_4, 5.8 KCl, 1.3 CaCl, 0.9 MgCl, 10 HEPES, 2 Na-pyruvate, and 5.6 D-glucose; vitamins and amino acids for Eagle's minimal essential medium were added from concentrates (Life Technologies, Paisley, UK), pH was adjusted to 7.4 at 310 mOsm. Whole-cell current- and voltage-clamp recordings were made from mid or apical P6-P11 mouse IHCs. The pipette solution contained (mM): 140 KCl, 3 $MgCl_2$, 1 EGTA-KOH, 5 Na_2ATP, 5 HEPES and 0.3 Na_2GTP, pH 7.4, and osmolarity of 295 mOsm. Pipette calcium buffers were chosen based on (2) where action potential kinetics made in whole-cell recordings with 1 mM EGTA matched those made in cell attached mode. For current-lamp recordings current was injected in 2–10 pA steps to determine the minimum current required to initiate action potential firing. IHCs started to fire action potentials when depolarized to -53 ± 0.4 mV ($n = 44$) and this threshold was used for all subsequent action potential recordings. For all recordings strychnine (100 nM, Sigma-Aldrich, Gillingham, UK) was added to the bath solution to block the $\alpha 9/\alpha 10$ acetylcholine receptor channel (AChR) to prevent spontaneous inhibitory postsynaptic potentials.

Ryanodine 1, 20, or 100 μM (Sigma-Aldrich, UK; Ascent Scientific, Cambridge, UK; Calbiochem, UK; or Biomol, UK) was used to enhance or block CICR, respectively. Ryanodine was added to the pipette solution to minimize any presynaptic effects either on the efferent fibers or directly on the AChR. A minimum of 5 min was allowed for the ryanodine to dialyze into the cell before the recording of any action potentials for analysis.

Data were acquired using an EPC10-F amplifier, sampling rate of 20 kHz, and PatchMaster v2.20 (HEKA Elektronik – Dr. Schulze GmbH, Lambrecht/Pfalz, Germany). Action potential analysis was performed using the Mini Analysis Program (Synaptosoft, Decatur, GA). In current-clamp experiments, the initiation of the current injection step sometimes triggered an initial action potential but this was disregarded from the data analysis as it is from a more hyperpolarized voltage and potentially contaminated with the voltage change due to current injection. Consequently, in each current-clamp experiment, the first action potential was considered to be the first one from baseline during current injection. Repolarization times were calculated from the peak of the action potential to 90% repolarization time to baseline. Prolonged action potential waveforms were defined as repolarization time $>$ mean $\pm 2\times$ SD of control experimental values. AHP amplitudes were measured from the baseline before the action potential to the lowest point of the AHP. Interspike interval was measured as the time between AP peaks, for prolonged oscillations the initial peak is taken.

Statistical analysis

Statistical comparisons were made by one-way analysis of variance nonparametric Kruskal Wallis test for non-Gaussian distributed populations and a Dunn's posttest comparison, values $p < 0.05$ indicating statistical significance. GraphPad Prism 4 was used for all statistical calculations. Data are presented as mean $\pm$ standard error of the mean (SE) unless otherwise stated. *N* numbers refer to the numbers of cells used.

Calcium imaging

Calcium imaging was carried out as described previously (25,28) at near body temperature 34–36°C. Briefly, cells were loaded with the cell-impermeable form of Fluo-4 (100 μM; Molecular Probes, Eugene, OR) through the patch pipette during whole-cell recording. Confocal images were collected in line scan mode (1–2 ms per line) using an Olympus FV300 confocal microscope (Olympus UK). Fluorescence was excited with 488 nm. Emitted light at wavelengths >515 nm were detected by the photomultiplier of the confocal system. Images were imported into Igor Pro v6 and bands of adjacent pixels corresponding to a band of cytoplasm nominally 1 μm wide were analyzed. For presentation the confocal line-scan image has been cropped using ImageJ.

Measurement of changes in membrane capacitance

Changes in membrane capacitance (ΔC_m) were measured using the track-in circuitry of the Optopatch amplifier (Cairn Instruments, Faversham, UK) (15,29). In brief, a 3 kHz sine wave (amplitude 34 mV) was applied to IHCs about the holding potential of -84 mV using the internal oscillator of the Optopatch. The sine wave is large enough to reveal changes in capacitance without itself activating any membrane currents because accurate measurement of membrane capacitance requires a high and constant membrane resistance (R_m). The command sine wave was interrupted for the duration of the voltage step, which was between 10 and 100 ms to nominally -5 mV. The capacitance signal from the Optopatch was amplified ($\times 50$), and filtered at 200 Hz externally using an 8-pole Bessel filter (NPI LPBS 08, NPI electronics, Haldenstrasse, Germany). Data were collected using pClamp software with a sampling frequency of 50 kHz. Membrane potentials were corrected for residual series resistance and liquid junction

potential and data analyzed using Origin6 software (OriginLab, Northampton, MA). Changes in membrane capacitance were measured by averaging the C_m trace over a 300 ms period following the stimulus and compared to the prestimulus baseline, which was set to zero using an average of 30 ms in the prestimulus trace. Statistical analysis as described previously.

Mathematical model

The model (see the Supporting Material for full model details), henceforth referred to as the IHC model, was originally proposed in (26) where it is shown that the model can reproduce complex firing patterns in a reasonable quantitative and qualitative agreement with experimental observations of IHC. In this work, we focus on the boundaries of existence and observability of such firing patterns, and we explore their dependence on CICR, which was previously unexplored.

For the purposes of our analysis, the IHC model was explored numerically with two techniques: time stepping (i.e., initial value problem numerical integration of the model equations) and numerical bifurcation continuation (using a boundary value problem approach, which provides better handling of numerical error). Time stepping was performed by specifying values for the control parameters, prescribing a set of initial conditions for the state variables, and then evolving them in time according to Eqs. S1–S4 (Supporting Material) using the XPPAUT (30) adaptive solver CVODE recommended for stiff system.

Once a periodic firing pattern is obtained with time-stepping simulations, it is possible to investigate its dependence upon control parameters using numerical bifurcation analysis (31). This approach reveals whether a given firing pattern is stable (therefore robust to small perturbations and observable experimentally), how it changes when control parameters are varied and how new periodic patterns are generated at critical points (called bifurcations).

Time stepping and bifurcation analysis are complementary techniques, because states found with the latter can be used as initial conditions for the former and vice versa. The final result is a comprehensive atlas (landscape) of solutions supported by the IHC model, which was used to characterize the behavior of the system and predict the occurrence of new firing patterns.

Numerical integration of the IHC model was done in XPPAUT (30), using the CVODE-solver with standard tolerance and adaptive time steps, whose default value was set to dt = 0.01 s. The bifurcation analysis was carried out using numerical continuation in AUTO (32). We set the number of mesh intervals used for discretization NTST = 400; the number of Gauss collocation points per mesh interval NCOL = 4; and the relative convergence criteria for equation parameters in the Newton/Chord method EPSL = 10^{-5} and EPSU = 10^{-5} for the tolerances of the Newton solver.

RESULTS

Action potential waveform is dependent on calcium release

Developing hair cells can fire calcium-based action potentials until the end of the second postnatal week, just before the onset of hearing (33). The calcium signal generated is likely to be critical in determining the overall shape and frequency of firing of the action potential as repolarization and maintenance of action potential firing is heavily reliant on the activation of the small conductance calcium-activated potassium current (SK2) current (4).

We have investigated the contribution of calcium release from intracellular stores on the action potential waveform and firing rate using ryanodine to either enhance (1 μM ryanodine) or inhibit (100 μM ryanodine) release of calcium from intracellular stores (24).

As shown recently, ryanodine is a positive modulator of the $\alpha9\alpha10$ AChR (34). Therefore, in all action potential recordings, extracellular strychnine (100 nM) was present in the bath solution, both for blocking AChR-ryanodine interactions and for preventing spontaneous inhibitory postsynaptic potentials, known to cause hyperpolarization and modulate action potential firing (2,4,8,35). In addition, ryanodine was applied intracellularly via the patch pipette to minimize any effects on cells surrounding IHCs including neurons.

Under our recording conditions at P6-10 cells were not firing spontaneous action potentials so a series of small depolarizing current injections were used to establish the threshold for firing (see Materials and Methods). This was determined to be −53 mV ± 0.4 ($n = 44$). During current injections cells from P6-8 mice fired trains of action potentials with variable frequency. Repolarization times were analyzed for all action potentials recorded from controls (794 action potentials, $n = 7$, analysis here does not include cells loaded with Fluo-4 for calcium imaging) and cells with either 1 μM (351 action potentials, $n = 6$) or 100 μM (751 action potentials, $n = 6$) intracellular ryanodine. Under control conditions the first action potential in a train had a repolarization time of 3.6 ± 0.17 ms (Fig. 1 *b*) with a gradual slowing in repolarization over the course of a recording, with a maximum slowing of ~20% (see Fig. 1 *d*). In addition, in two of seven control experiments some prolonged action potentials were seen (22/794 action potentials) (defined as repolarization time > mean ± 2 SD of control experiment values). As development progressed toward the end of the second postnatal week, prolonged action potentials became more frequent with 40% of cells showing prolonged action potentials at P10 ($n = 25$).

Enhancing CICR (1 μM ryanodine) had no effect on action potential amplitude and did not significantly reduce the repolarization time of the first action potential in a train (3.31 ± 0.11 ms, $n = 6$ cells) compared to control (3.6 ± 0.17 ms, $n = 7$ cells) (Fig. 1 *b*). However, analysis of all action potentials revealed that, overall, repolarization was significantly faster in the presence of 1 μM ryanodine (4.02 ± 0.03 ms, $n = 6$ cells, $p < 0.001$) compared to control action potentials (4.54 ± 0.1 ms, $n = 7$ cells) (Fig. 1 *c*). Recordings in the presence of 1 μM ryanodine showed no prolonged action potentials (0/351, $n = 6$) and less variation in action potential duration with an SD of ±0.6 ms (coefficient of variation 15.75%) compared to control SD of ±2.7 ms (coefficient of variation 59.49%). The averaged data of the first 10 action potentials in a train show that there was no effect on the progressive slowing of repolarization, which remained similar to control values at 20% (Fig. 1 *d*).

In contrast, when CICR was blocked with 100 μM ryanodine, the repolarization time for the first action potential in a train was significantly slower than in control (3.6 ± 0.17 ms, $n = 7$) compared to ryanodine (5.6 ± 0.4 ms, $n = 6$, $p < 0.001$). In addition, blocking CICR led to a significant

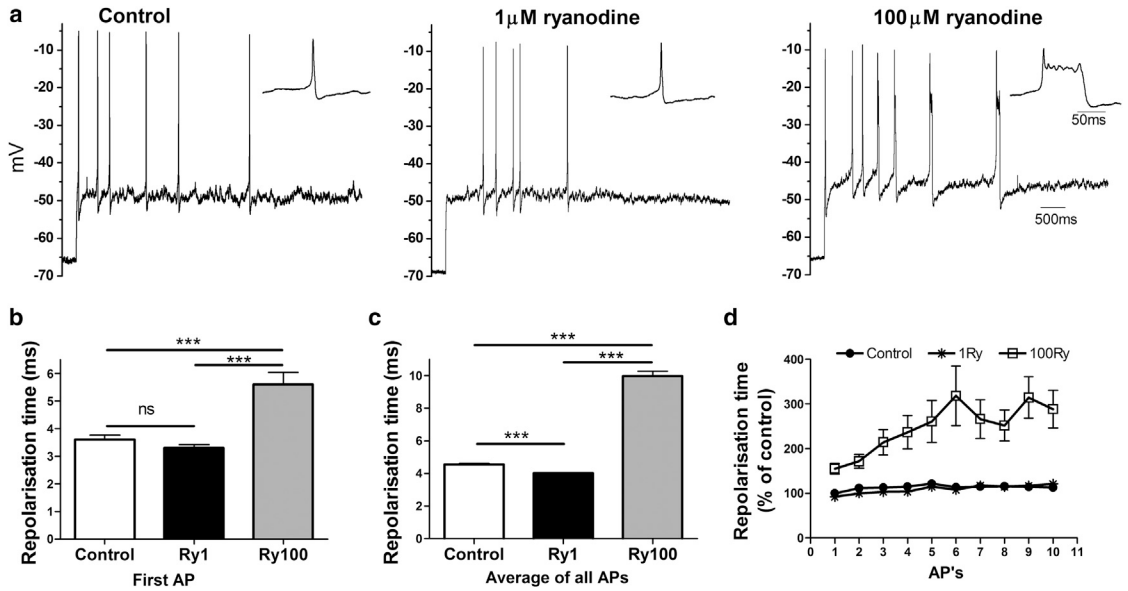

FIGURE 1 The effects of ryanodine on action potential firing. (*a*) Representative current-clamp recording of trains of action potentials in control, 1 μM (*enhancing CICR*) and 100 μM ryanodine (*blocking CICR*). Insets show the last action potential in the train in detail. 100 μM ryanodine slowed the first action potential and progressively slowed action potential repolarization during the train leading to prolonged plateaus. (*b*) Bar graph of averaged repolarization times of the first action potential in the train for each condition. (*c*) Bar graph of averaged repolarization time for all action potentials. (*d*) Line graph of averaged repolarization times for each of the first 10 action potentials in the three experimental conditions: control, 1 and 100 μm ryanodine. Data are presented as percentages normalized to the first action potential in the control condition. All bars are means $\pm$ SE. The level of significance is marked as $*p \leq 0.05$; $**p \leq 0.01$; $***p \leq 0.001$.

slowing of action potential repolarization during trains of action potentials (Fig. 1, *a* and *d*), leading to action potentials with prolonged waveforms (Fig. 1 *a*, *inset*). The average repolarization time slowed to (9.97 $\pm$ 0.3 ms, coefficient of variation 81.9%) (Fig. 1 *c*), with some action potentials as long as 75 ms (Figs. 1 *a* and 2 *a*). However, prolonged action potentials did eventually show a robust repolarization and AHP during recordings. Over the course of the six experiments a total of 204/751 action potentials were prolonged. These data show that a crucial part of the calcium signal during action potential firing is generated by calcium release from intracellular stores.

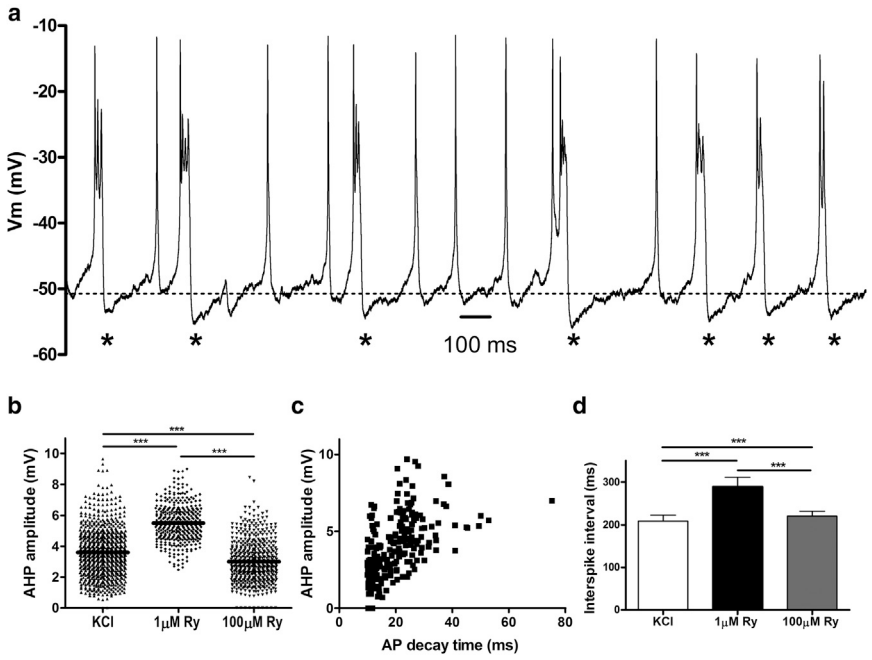

FIGURE 2 Blocking CICR produces complex patterns of firing. (*a*) Representative recording showing mixed pattern of brief and prolonged action potentials recorded in the presence of 100 μM ryanodine. Each asterisk marks a large AHP generated by a prolonged action potential. Dotted line represents the average potential from which action potential firing was generated in this example. (*b*) Analysis of the AHP for control, 1 and 100 μM ryanodine. Prolonged action potential AHPs were excluded from this analysis. (*c*) Plot of AHP amplitude verses the average decay time for all action potentials that were prolonged (greater than mean $\pm$2 SD). (*d*) Interspike interval for control, 1 and 100 μM ryanodine with prolonged action potentials removed from analysis. Data presented as means $\pm$ SEM. The level of significance is marked as $*p \leq 0.05$; $**p \leq 0.01$; $***p \leq 0.001$.

Time-stepping numerical simulations of the model (Eqs. S1–S4, Supporting Material) agree well with the experimental data reported previously. Decreasing the permeability of CICR channels (RyR2), represented by the parameter p_{ER} in the model, results in complex periodic solutions with prolonged action plateaus (see Fig. 3 *b*). This could be explained noting that reducing the release of calcium from the endoplasmic reticulum induces a decrease in intracellular calcium concentration. This effectively results in lower SK2 currents and is reminiscent of an apamin block of the IHCs SK2 channels (see Fig. 3 *C* in (4) and Fig. 2 *a* in (26)).We note that our model is a Chay-Keizer type of model (36) in which the voltage plateau is not explicitly included. Therefore, in the model the voltage plateau is an emergent property arising predominantly from the interactions between the voltage variable (V_m) and the activation of the delayed rectifier-type potassium current (n) (37).

Blocking calcium release causes mixed patterns of action potential waveforms

Information during action potential firing can be encoded for by both frequency of firing and action potential shape, leading to calcium signals with a wide range of spatial and temporal characteristics (38,39). In our experiments, although the effect of blocking CICR tended to cause a progressive slowing of action potential repolarization, in many experiments more complex behavior with a mix of shorter and prolonged action potentials were seen (Fig. 2 *a*, prolonged action potentials are marked with an *asterisk*). These prolonged action potentials did eventually repolarize and were always followed by a robust AHP, much larger than seen for the shorter action potentials in the same recording.

Analysis of the AHP from action potentials that were not prolonged in each experimental condition showed that enhancing CICR produced significantly larger AHPs than in control conditions (1 μM ryanodine: 5.5 $\pm$ 0.07 mV, control: 3.6 $\pm$ 0.06 mV) and that blocking CICR significantly reduced the AHP (100 μM ryanodine: 3.0 $\pm$ 0.06 mV) (Fig. 2 *b*). For the prolonged action potentials, analysis showed that the length of the action potential correlated with the size of the AHP (Fig. 2 *c*), with longer action potentials generally leading to larger AHPs. In addition, we analyzed the interspike interval in all recordings. Enhancing CICR had a clear effect of significantly increasing the interspike intervals (control: 208 $\pm$ 14.5 ms, 1 μM ryanodine: 289 $\pm$ 21.9 ms) and thus slowing the firing rate. However, the results from blocking CICR are more difficult to interpret. If all action potentials were included in the analysis, the interspike interval was then significantly longer than in control (234 $\pm$ 9.9 ms) due to the prevalence of prolonged action potentials. Removal of those action potentials

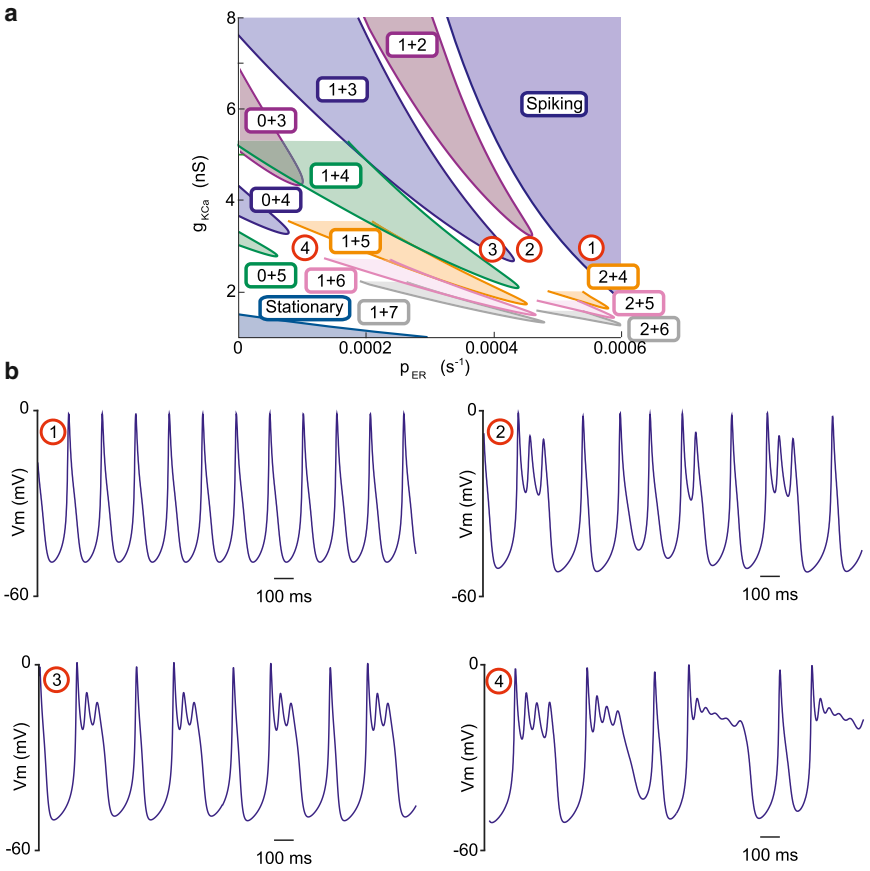

FIGURE 3 Firing patterns obtained with numerical simulations of the IHC model. (*a*) Results of numerical bifurcation analysis of the IHC model. The graph shows a landscape of possible firing patterns occurring when the CICR rate (p_{ER}) and the SK2-channel conductance (g_{KCa}) are varied. Patterns are classified according to their number of large and prolonged spikes with small plateau oscillations (for instance 1+3 stands for 1 large spike followed by a prolonged spike with 3 small plateau oscillations). Shaded areas correspond to values of parameters where stable periodic oscillations are found. If the parameters are chosen in one of the white areas, irregular mixed firing patterns then occur. (*b*) Examples of firing patterns obtained with time-stepping simulations. Model parameters are chosen in the Spiking area (*label 1*) giving rise to a purely spiking periodic pattern. If the CICR rate is decreased (while the SK2-channel conductance is kept at a constant value), an aperiodic mixed pattern is found (*label 2*). Decreasing the CICR further leads to a regular periodic 1+3 pattern (*label 3*) and a further mixed pattern (*label 4*). The shape of the aperiodic patterns (*labels 2* and *4*) is influenced by their position on the (pER, gKCa)-plane.

classified as prolonged (mean in control conditions ± 2 SD) reduced interspike interval to 219 ± 12.4 ms, but this remained significantly longer than control conditions. This difference may be due to the broad range of action potential durations present in these experiments and the chaotic nature of the firing, and because the relationship between the size of the AHP and the interspike interval may be more complex in the presence of 100 μM ryanodine. These data show that CICR has a pivotal role in shaping both action potential shape and modulating firing rate. We suggest that prolonged action potentials could occur physiologically if the amount of calcium release from the stores were to change during repetitive firing.

The occurrence of mixed patterns of action potentials (spikes) was also investigated numerically using both time-stepping and numerical bifurcation analysis. The IHC model was first evolved in time, setting parameters as in Table S1, and then numerical bifurcation analysis was conducted for two control parameters: the CICR rate (p_{ER}), which influences the calcium signal in Eq. S4 (Supporting Material), and the conductance of the SK2 channels ($g_{K(Ca)}$), which in turn regulates the SK2 current in Eq. S1 (Supporting Material). This analysis allows us to assemble an atlas of IHC model solutions by tracing the bifurcations that give rise to stable periodic solutions because the two control parameters of interest, namely p_{ER} and $g_{K(Ca)}$, are varied. Decreasing p_{ER} in the model corresponds to blocking CICR via ryanodine, whereas reducing g_{KCa} mimics an experimental block by apamin (see Fig. 2 *a* in (26)).

Fig. 3 *a* reveals the existence of an intricate landscape of firing patterns, classified according to the number of large spikes and prolonged spikes with plateau oscillations. For example 1+3 denotes a pattern with a single large spike followed by a prolonged spike with three plateau oscillations (an example is shown in the *third panel* of Fig. 3 *b*). The landscape features nonoscillatory stationary states (labeled as *Stationary* in Fig. 3 *a*), as well as single-spike periodic solutions (labeled as *Spiking* in Fig. 3 *a*); periodic solutions without single spikes (labeled 0+3, 0+4, 0+5 in Fig. 3 *a*) and with an increasing number of large spikes and plateau oscillations (labeled 2+4, 2+5, 2+6 in Fig. 3 *a*). Shaded areas correspond to values of parameters where stable periodic (*complex*) oscillations exist: from a mathematical standpoint, mixed firing patterns are found to lie on isolas (*closed curves in parameter space*) and stability changes are associated with period-doubling bifurcations, which were traced in the (p_{ER}, g_{KCa})-plane and plotted as solid line curves in Fig. 3 *a*. The white areas in Fig. 3 *a* correspond to parameter regimes in the model where no stable periodic attractors could be detected. Time-stepping model simulations indicate that if the model parameters are chosen in one of the white areas, irregular mixed firing patterns then occur, as seen in our experiments with 100 μM ryanodine.

Examples of firing patterns for four different values of p_{ER} while keeping the value of $g_{K(Ca)}$ fixed were computed via time-stepping simulations and are shown in Fig. 3 *b*. These model simulations correspond to blocking CICR and indicate that this leads to complex spiking behavior with prolonged action potentials closely resembling the experimental recordings shown in Fig. 2 *a*. The first panel in Fig. 3 *b* shows regular spiking and represents typical model behavior for high values of p_{ER}. The irregular mixed firing patterns are composed of large (brief action potentials) spikes and prolonged action potentials (comprising small oscillations on top of a depolarized plateau) that alternate unpredictably as depicted in the second and forth panels of Fig. 3 *b*. A stable, periodically repeating firing pattern containing 1 large spike and 3 small plateau oscillations (1+3) is also illustrated in the third panel of Fig. 3 *b*. Note that we made use of such solutions to perform the systematic bifurcation analysis in the control parameters that we focus on in this study, namely p_{ER} and g_{KCa} (shown in Fig. 3 *a*).

Slight variations of the control parameters can induce dramatic changes in the firing patterns in close proximity to the boundaries depicted as solid line curves in Fig. 3 *a*. An example is shown in the second panel of Fig. 3 *b*: when the CICR rate is decreased to cross the boundary of the spiking region (a period-doubling bifurcation), the action potential changes from a purely spiking to an aperiodic mixed firing pattern. When the CICR rate was decreased even further, a regular periodic 1+3 firing pattern emerged (illustrated in the *third panel* of Fig. 3 *b*) as we entered the corresponding shaded area, followed by periodic 1+4 and 1+5 patterns (not shown) and a second aperiodic mixed firing pattern (depicted in the *fourth panel* of Fig. 3 *b*).

Complex action potentials waveforms generate oscillating calcium signals

We used simultaneous confocal line-scan imaging and current-clamp recordings to investigate the calcium signals during normal and prolonged action potentials. The image in Fig. 4 shows an example line-scan image across the basal pole of a P10 IHC during action potential firing initiated by a small current injection (see Materials and Methods) under normal conditions. Analysis of the line-scan image in a band, nominally 1 μm wide, adjacent to the plasma membrane reveal the fluorescence changes during action potential firing (Fig. 4 *b*, *middle trace*). During brief action potentials calcium signals were very transient in nature. In comparison, prolonged action potentials often showed initial oscillations in membrane potential that then became sustained depolarizations. As expected, the corresponding calcium signals matched these observations closely demonstrating that the calcium signal generated can follow the slow oscillations in membrane voltage and last throughout the duration of the plateau phase of the action potential. These larger calcium signals may explain how the prolonged action potentials eventually show robust repolarization. Although many

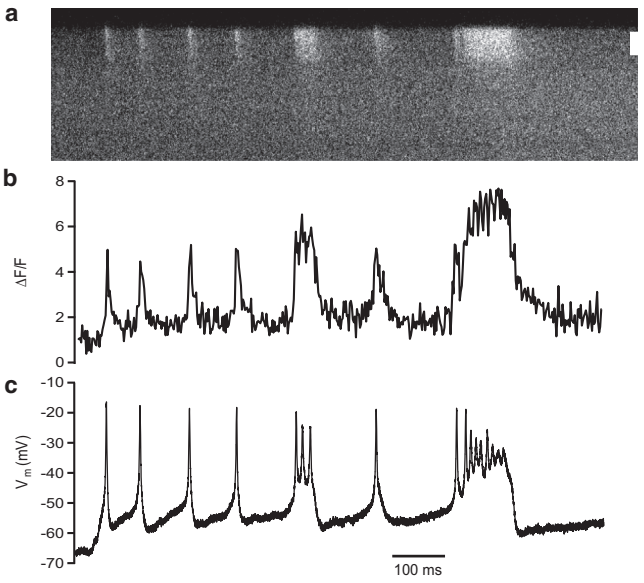

FIGURE 4 Calcium signals during normal and prolonged action potential firing. (*a*) Line-scan image taken through the basal pole of a P10 IHC in control conditions. Fluorescence changes show increases of intracellular calcium during action potential recording. (*b*) Analysis of fluorescence (indicated by the *white bar* superimposed on the image) measured from a nominally 1 μm band of cytoplasm near the plasma membrane data ($\Delta F/F$) are normalized to prestimulus levels. (*c*) Simultaneous recording of membrane potential showing both brief and oscillating action potential waveforms.

calcium channels and SK2 channels are closely located, when the calcium signal spreads it is likely that SK2 channels further away are also activated, thus eventually activating sufficient SK2 channels to promote repolarization of the action potential and generate the large AHP (Fig. 4 *a*). It is important to note that the prolonged waveform solutions in the model are also associated with a larger increase in the calcium signal (see Fig 2 *a* in (26)). This is expected and again consistent with the experimental results described previously and shown in Fig. 4.

The effect of CICR on exocytosis

In the mature peripheral auditory system calcium influx and exocytosis are tightly coupled (15) and there is no role for CICR (40). However, in the immature system, exocytosis and calcium influx are less tightly coupled (15). Nevertheless, it is essential that action potential firing generates sufficient transmitter release to drive spiking in developing spiral ganglion neurons (41,42). We investigated whether CICR could have a role in boosting the calcium signal that triggers exocytosis before the onset of hearing, when coupling between calcium entry a transmitter release is less robust (15,43). Cells that were voltage clamped to −84 mV and step depolarizations to nominally −5 mV for between 10 and 100 ms were used to activate calcium influx and the resulting increases in capacitance were measured. Fig. 5 *a* shows experimental recordings of capacitance changes in response to repeated steps to −5 mV for 100 ms with a 1 s interstimulus interval (for clarity only the first 5 steps are shown). The initial depolarization was always the largest with a subsequent decline in exocytosis over the following depolarizations to a steady value of ~20 fF, an effect that would fully recover after a 1 min interval. The average data (n = 19) from these experiments is plotted in Fig. 5 *b*, where all 10 stimuli are plotted and the decline in capacitance release to repeated depolarizations is fit with a single exponential time course. We then tested the effects of three different concentrations of ryanodine: 1 μM (n = 6), 20 μM (n = 6), or 100 μM (n = 13) on the capacitance change following repeated stimuli to nominally −5 mV for 10, 20, 50, or 100 ms. In all experimental conditions depolarizations were carried out either sequentially for 10 steps for one time period, e.g., 100 ms, or randomly for 10, 20, 50, or 100 ms and compared to experiments carried out in the same way in control conditions. The data presented in Fig. 5 *c* are averages ± SE of the response to depolarization of 10, 20 50, and 100 ms in control, 1 μM ryanodine, 20 μM ryanodine, or 100 ryanodine μM. Our data are in agreement with other groups where longer depolarizations lead to statistically significant increases in exocytosis (14,15). However, we found no effect of

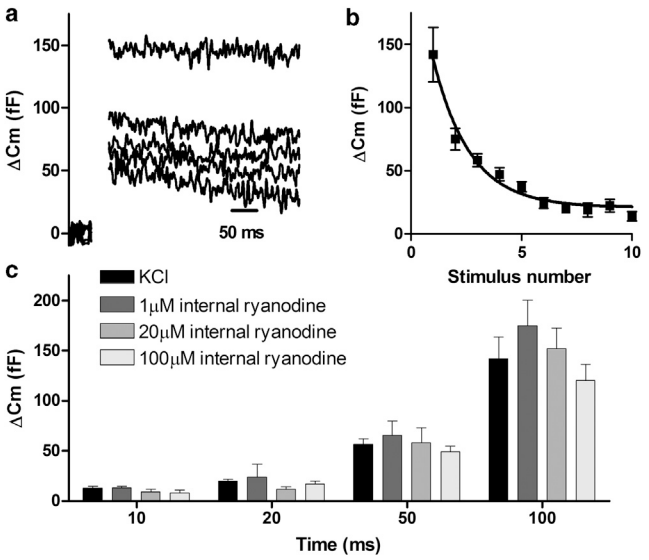

FIGURE 5 The effects of ryanodine on neurotransmitter release from IHCs. (*a*) Representative traces of membrane capacitance changes in a P7 mouse in response to a series of 100 ms depolarizations to nominally −5 mV, for clarity only 5 of 10 depolarizations are shown. (*b*) Average data from P7-8 mice for the series of 10 depolarizations (n = 19), error bars are SE. Data are fitted with a single exponential for the decline in capacitance response to successive depolarizations. (*c*) Bar graph of capacitance responses to control (n = 19), 1 μM ryanodine (n = 6), 20 μM ryanodine (n = 6), and 100 μM ryanodine (n = 13) in the pipette. The effects of ryanodine were tested for depolarizations to nominally −5 mv for 10, 20, 50, and 100 ms, with the length of depolarizations given in a random order with a 1 s interval between depolarizations.

ryanodine at any concentration, either to the response to single depolarizations (Fig. 5 *c*) or in the capacitance decline during a series of 10 depolarizations (data not shown). These data suggest that CICR is not involved in generating the calcium signal that directly triggers exocytosis in immature hair cells. However, CICR does have an important role in exocytosis as it modulates both action potential shape and the firing pattern, which are the physiological stimuli for driving transmitter release and thus guiding development of higher auditory pathways.

DISCUSSION

It is generally accepted that much of the complex auditory circuitry is established before the onset of hearing and is therefore independent of sound-evoked activity (21,44). During the prehearing developmental phase IHCs generate calcium-based action potentials (1,7) that trigger transmitter release onto developing spiral ganglion neurons, generating bursts of action potentials that have been proposed to be important in establishing the neuronal circuits (17,41,45).

Because the action potential waveform is dependent on the activation of a calcium-sensitive potassium current, SK2 (4), both the kinetics of the action potential and the amount of transmitter release are dependent on the intracellular calcium signal generated during IHC firing. The aim of this study was to determine whether CICR was an essential component of this calcium signal. The information gained not only shows the functional role for CICR in developing IHCs, but also provides important insights into the calcium signaling mechanisms involved in early developmental processes.

CICR in action potential firing

In neonatal IHCs SK2 currents are essential for the fast repolarization and maintenance of action potential firing (4–6). Our data are in good agreement with action potentials recorded by other groups under similar experimental conditions (7,8,14). In our experiments 100 μM ryanodine was used to block CICR thus reducing the size and spread of the calcium signal (25). We demonstrated that blocking CICR slowed the rate of repolarization of the first action potential in a train, and also produced a cumulative slowing during repetitive firing leading to very prolonged action potentials, and often produced complex patterns with mixed firing rates. In our model, we have already shown in (26) that decreasing the SK2 current in the model prolongs the action potential firing by effectively slowing down the Ca^{2+} component of the periodic solutions found in the model (Eqs. S1–S4, Supporting Material). Hence, the trajectory spends more and more time in a region of phase space where Ca^{2+} is high, thereby generating prolonged action potentials. The effects of blocking CICR are somewhat similar, but less dramatic, than those seen for blocking SK2 with apamin (4), because blocking CICR does not abolish the calcium signal, it merely reduces it (25), thus some activation of the SK2 current will remain under our conditions. In contrast, enhancing CICR-generated action potentials with less variation in duration, and an absence of any prolonged action potentials, suggests a more consistent activation of SK2.

As well as action potential shape, firing patterns were also altered by changing CICR. Enhancing CICR increased the AHP and slowed the firing rate. During mixed firing, brief action potentials had a reduced AHP compared with control. In contrast, prolonged action potentials generated large long-lasting AHPs temporarily reducing the firing rate by increasing the interspike interval. The firing pattern switched between brief and prolonged action potentials and we suggest that this is due to the balance between the resting calcium level, CICR, and the amount of SK2 activation. Such complex firing patterns have not been reported previously in IHCs, but we have used mathematical models to predict the effects of a reduction in SK2 current and our model predicts mixed firing patterns (26). Here, we analyzed the model with particular focus on the interaction between CICR and activation of SK2 channels. Using numerical continuation we characterized the effects of varying both SK2 channels conductance as well as CICR rate on the pattern of electrical activity in the model. Furthermore, we showed that a characteristic ladder of attractors (which give rise to the complex behavior observed experimentally) occurs robustly, in a relatively large portion of parameter space.

Together, these data clearly show that CICR is an essential component of the calcium signal that is responsible for the effective repolarization of action potentials and timing of action potential firing.

Modulation of transmitter release

In the immature animal, the calcium dependence of the synapse and size of calcium current have not yet reached their mature level (15,43). Our measurements of cell capacitance demonstrated that, similar to the case in adults (40), there is no direct contribution of CICR to the intracellular calcium signal that triggers transmitter release, either during short or long depolarizations. The lack of any contribution from intracellular stores, to increases in cell capacitance in the immature animal, indicates that the calcium source (channel) and calcium-dependent sites that are involved in triggering transmitter release are already localized as they are in the adult (40). This suggests that the calcium signals involved in transmitter release and action potential firing in immature hair cells are segregated. Such localization of calcium signals is a hallmark of calcium signaling in many systems (46) and is due to physical separation of the mechanisms involved as well as regulatory mechanisms such as calcium buffering and extrusion mechanisms.

Despite the lack of direct effect of calcium release on transmitter release, it is well established that action potentials generate transmitter release and that the amount of release is highly dependent on the length of the depolarization (14,15). Therefore, CICR has an indirect role in maintaining transmitter release in immature IHCs because it sets the action potential kinetics and thus controls the length of the depolarizations that triggers transmitter release.

Generation of complex firing patterns

Unlike sodium action potentials, calcium-based action potentials that rely on calcium-activated currents for part of their repolarization phase (4) can be easily modulated physiologically by altering CICR and thus the calcium signal, resulting in trains of action potentials with different kinetics (Fig. 2). Numerical simulations of the IHC model support this observation, because they show that changes of the CICR rate in the model induce abrupt transitions in the action potential time profiles. Such transitions involve both regular periodic firing patterns and mixed firing states. Our numerical bifurcation analysis reveals that generically, during complex bursting, the SK2 channels conductance controls the number of small plateau oscillations (the lower g_{KCa}, the higher the number of plateau oscillations), whereas a large contribution from CICR promotes normal spiking behavior (the higher p_{ER}, the higher the number of large spikes). Such complex firing patterns have been observed in developing neurons (47). A generation of mixed action potential firing would produce both small transient calcium signals and larger, long-lasting signals capable of spreading to the nucleus where they may affect gene transcription pathways (48) potentially impacting on the intrinsic development of the hair cell. In addition, prolonged action potentials would lead to longer bursts of transmitter release potentially affecting the early experience-independent firing in auditory neurons.

To our knowledge, the occurrence of the complex firing patterns in the model that correspond to large spike(s) + plateau (oscillation(s)) bursting attractors have not been observed in this type of model so far. This type of solution in our model may result from interactions between Ca^{2+}-dependent inactivation of Cav1.3 calcium channels and/or the double-exponential inactivation function for the delayed-rectifier K^+ channels included in the model on one hand, and the activation of Cav1.3 calcium channels combined with the rate of CICR on the other. Numerical analysis of possible interactions governing the dynamical nature of complex firing patterns in the model would be a very interesting future direction for the theoretical part of this research; however, it is beyond the scope of this study.

It is obvious that action potential firing requires calcium signals that are robustly generated yet tightly regulated. Any defect in the mechanisms for generating or regulating such precise calcium signaling could lead to a disruption in action potential; consequently; firing could affect the development of the auditory system. Such remodeling of calcium signals during disease is known to occur in cardiac myocytes that rely heavily on CICR to generate their calcium signals, as well as underlying neurological disease such as Alzheimer's disease (38,39,49). Understanding how immature IHC action potentials are shaped and regulated and the mechanisms that underlie these properties gives us greater insight into how such events may contribute to neuronal circuits and intrinsic development and more widely to understand how complex behaviors in other systems may be generated.

SUPPORTING MATERIAL

Supporting Materials and Methods, one figure, and one table are available at http://www.biophysj.org/biophysj/supplemental/S0006-3495(15)00082-X.

ACKNOWLEDGMENTS

H.K. and R.I. were supported by grant 072809/Z/03/Z from the Wellcome Trust. L.G. was supported by a PhD position funded by the University of Bristol. D.A. was partially supported by grant EP/E032249/1 from the Engineering and Physical Sciences Research Council (EPSRC) and K.T.-A. by EPSRC grants EP/I018638/1 and EP/L000296/1. The authors declare no competing financial interests.

SUPPORTING CITATIONS

References (50–53) appear in the Supporting Material.

REFERENCES

1. Kros, C. J., J. P. Ruppersberg, and A. Rüsch. 1998. Expression of a potassium current in inner hair cells during development of hearing in mice. *Nature.* 394:281–284.
2. Johnson, S. L., T. Eckrich, …, W. Marcotti. 2011. Position-dependent patterning of spontaneous action potentials in immature cochlear inner hair cells. *Nat. Neurosci.* 14:711–717.
3. Roux, I., E. Wersinger, …, E. Glowatzki. 2011. Onset of cholinergic efferent synaptic function in sensory hair cells of the rat cochlea. *J. Neurosci.* 31:15092–15101.
4. Marcotti, W., S. L. Johnson, and C. J. Kros. 2004. A transiently expressed SK current sustains and modulates action potential activity in immature mouse inner hair cells. *J. Physiol.* 560:691–708.
5. Johnson, S. L., J. P. Adelman, and W. Marcotti. 2007. Genetic deletion of SK2 channels in mouse inner hair cells prevents the developmental linearization in the Ca2+ dependence of exocytosis. *J. Physiol.* 583:631–646.
6. Marcotti, W., S. L. Johnson, …, C. J. Kros. 2003. Developmental changes in the expression of potassium currents of embryonic, neonatal and mature mouse inner hair cells. *J. Physiol.* 548:383–400.
7. Marcotti, W., S. L. Johnson, …, C. J. Kros. 2003. Sodium and calcium currents shape action potentials in immature mouse inner hair cells. *J. Physiol.* 552:743–761.
8. Glowatzki, E., and P. A. Fuchs. 2000. Cholinergic synaptic inhibition of inner hair cells in the neonatal mammalian cochlea. *Science.* 288:2366–2368.
9. Spitzer, N. C., N. J. Lautermilch, …, T. M. Gomez. 2000. Coding of neuronal differentiation by calcium transients. *BioEssays.* 22:811–817.

10. Dolmetsch, R. E., R. S. Lewis, …, J. I. Healy. 1997. Differential activation of transcription factors induced by Ca2+ response amplitude and duration. *Nature.* 386:855–858.

11. Dolmetsch, R. E., K. Xu, and R. S. Lewis. 1998. Calcium oscillations increase the efficiency and specificity of gene expression. *Nature.* 392:933–936.

12. West, A. E., W. G. Chen, …, M. E. Greenberg. 2001. Calcium regulation of neuronal gene expression. *Proc. Natl. Acad. Sci. USA.* 98:11024–11031.

13. Johnson, S. L., S. Kuhn, …, W. Marcotti. 2013. Presynaptic maturation in auditory hair cells requires a critical period of sensory-independent spiking activity. *Proc. Natl. Acad. Sci. USA.* 110:8720–8725.

14. Beutner, D., and T. Moser. 2001. The presynaptic function of mouse cochlear inner hair cells during development of hearing. *J. Neurosci.* 21:4593–4599.

15. Johnson, S. L., W. Marcotti, and C. J. Kros. 2005. Increase in efficiency and reduction in Ca2+ dependence of exocytosis during development of mouse inner hair cells. *J. Physiol.* 563:177–191.

16. Glowatzki, E., and P. A. Fuchs. 2002. Transmitter release at the hair cell ribbon synapse. *Nat. Neurosci.* 5:147–154.

17. Tritsch, N. X., A. Rodríguez-Contreras, …, D. E. Bergles. 2010. Calcium action potentials in hair cells pattern auditory neuron activity before hearing onset. *Nat. Neurosci.* 13:1050–1052.

18. Stellwagen, D., and C. J. Shatz. 2002. An instructive role for retinal waves in the development of retinogeniculate connectivity. *Neuron.* 33:357–367.

19. Leão, R. N., M. M. Naves, …, B. Walmsley. 2006. Altered sodium currents in auditory neurons of congenitally deaf mice. *Eur. J. Neurosci.* 24:1137–1146.

20. Leao, R. N., H. Sun, …, B. Walmsley. 2006. Topographic organization in the auditory brainstem of juvenile mice is disrupted in congenital deafness. *J. Physiol.* 571:563–578.

21. Kandler, K., A. Clause, and J. Noh. 2009. Tonotopic reorganization of developing auditory brainstem circuits. *Nat. Neurosci.* 12:711–717.

22. Platzer, J., J. Engel, …, J. Striessnig. 2000. Congenital deafness and sinoatrial node dysfunction in mice lacking class D L-type Ca2+ channels. *Cell.* 102:89–97.

23. Endo, M., M. Tanaka, and Y. Ogawa. 1970. Calcium induced release of calcium from the sarcoplasmic reticulum of skinned skeletal muscle fibres. *Nature.* 228:34–36.

24. Meissner, G. 1986. Ryanodine activation and inhibition of the Ca2+ release channel of sarcoplasmic reticulum. *J. Biol. Chem.* 261:6300–6306.

25. Kennedy, H. J., and R. W. Meech. 2002. Fast Ca2+ signals at mouse inner hair cell synapse: a role for Ca2+-induced Ca2+ release. *J. Physiol.* 539:15–23.

26. Szalai, R., K. Tsaneva-Atanasova, …, N. P. Cooper. 2011. Nonlinear models of development, amplification and compression in the mammalian cochlea. *Philos. Transact. A Math. Phys. Eng. Sci.* 369:4183–4204.

27. Johnson, S. L., and W. Marcotti. 2008. Biophysical properties of CaV1.3 calcium channels in gerbil inner hair cells. *J. Physiol.* 586:1029–1042.

28. Kennedy, H. J. 2002. Intracellular calcium regulation in inner hair cells from neonatal mice. *Cell Calcium.* 31:127–136.

29. Johnson, S. L., M. V. Thomas, and C. J. Kros. 2002. Membrane capacitance measurement using patch clamp with integrated self-balancing lock-in amplifier. *Pflugers Arch.* 443:653–663.

30. Ermentrout, B. 2002. Simulating, Analyzing, and Animating Dynamical Systems: A Guide to XPPAUT for Researchers and Students. Society for Industrial & Applied Mathematics, Philadelphia, PA, [Sunbury-on-Thames: Electronica Books & Media].

31. Allgower, E. L., and K. Georg. 2003. Introduction to Numerical Continuation Methods. Classics in Applied Mathematics. Society for Industrial and Applied Mathematics, Philadelphia, PA, p. 388.

32. Doedel, E. J. 1981. AUTO: a program for the automatic bifurcation analysis of autonomous systems, in Congr Numer.265–284.

33. Johnson, S. L., H. J. Kennedy, …, W. Marcotti. 2012. The resting transducer current drives spontaneous activity in prehearing mammalian cochlear inner hair cells. *J. Neurosci.* 32:10479–10483.

34. Zorrilla de San Martín, J., J. Ballestero, …, P. A. Fuchs. 2007. Ryanodine is a positive modulator of acetylcholine receptor gating in cochlear hair cells. *J. Assoc. Res. Otolaryngol.* 8:474–483.

35. Goutman, J. D., P. A. Fuchs, and E. Glowatzki. 2005. Facilitating efferent inhibition of inner hair cells in the cochlea of the neonatal rat. *J. Physiol.* 566:49–59.

36. Chay, T. R., and J. Keizer. 1983. Minimal model for membrane oscillations in the pancreatic beta-cell. *Biophys. J.* 42:181–190.

37. Sherman, A., and R. Bertram. 2005. Integrative modeling of the pancreatic β-cell. *In* Encyclopedia of Genetics, Genomics, Proteomics and Bioinformatics. Vol. 3. Proteomics. M. Dunn, editor. Wiley-VCH, Chichester, UK, p. 116.

38. Berridge, M. J. 2012. Calcium signalling remodelling and disease. *Biochem. Soc. Trans.* 40:297–309.

39. Berridge, M. J. 2006. Remodelling Ca2+ signalling systems and cardiac hypertrophy. *Biochem. Soc. Trans.* 34:228–231.

40. Frank, T., D. Khimich, …, T. Moser. 2009. Mechanisms contributing to synaptic Ca2+ signals and their heterogeneity in hair cells. *Proc. Natl. Acad. Sci. USA.* 106:4483–4488.

41. Tritsch, N. X., E. Yi, …, D. E. Bergles. 2007. The origin of spontaneous activity in the developing auditory system. *Nature.* 450:50–55.

42. Tritsch, N. X., and D. E. Bergles. 2010. Developmental regulation of spontaneous activity in the Mammalian cochlea. *J. Neurosci.* 30:1539–1550.

43. Beutner, D., T. Voets, …, T. Moser. 2001. Calcium dependence of exocytosis and endocytosis at the cochlear inner hair cell afferent synapse. *Neuron.* 29:681–690.

44. Friauf, E., and C. Lohmann. 1999. Development of auditory brainstem circuitry. Activity-dependent and activity-independent processes. *Cell Tissue Res.* 297:187–195.

45. Blankenship, A. G., and M. B. Feller. 2010. Mechanisms underlying spontaneous patterned activity in developing neural circuits. *Nat. Rev. Neurosci.* 11:18–29.

46. Berridge, M. J. 2006. Calcium microdomains: organization and function. *Cell Calcium.* 40:405–412.

47. Cherubini, E., M. Griguoli, …, L. Lagostena. 2011. The depolarizing action of GABA controls early network activity in the developing hippocampus. *Mol. Neurobiol.* 43:97–106.

48. Bengtson, C. P., and H. Bading. 2012. Nuclear calcium signaling. *Adv. Exp. Med. Biol.* 970:377–405.

49. Berridge, M. J. 2011. Calcium signalling and Alzheimer's disease. *Neurochem. Res.* 36:1149–1156.

50. Hodgkin, A. L., and A. F. Huxley. 1952. A quantitative description of membrane current and its application to conduction and excitation in nerve. *J. Physiol.* 117:500–544.

51. Grant, L., and P. Fuchs. 2008. Calcium- and calmodulin-dependent inactivation of calcium channels in inner hair cells of the rat cochlea. *J. Neurophysiol.* 99:2183–2193.

52. Tarabova, B., L. Lacinova, and J. Engel. 2007. Effects of phenylalkylamines and benzothiazepines on Ca(v)1.3-mediated Ca2+ currents in neonatal mouse inner hair cells. *Eur. J. Pharmacol.* 573:39–48.

53. Zampini, V., S. L. Johnson, …, W. Marcotti. 2010. Elementary properties of CaV1.3 Ca(2+) channels expressed in mouse cochlear inner hair cells. *J. Physiol.* 588:187–199.